# P1.1 Mesoscale Predictability Estimated through Explicit Simulation of Moist Baroclinic Waves

**Zhe-Min Tan[1, 2], Richard Rotunno[2], Chris Snyder[2] and Fuqing Zhang[3]**

*1. Department of Atmospheric Sciences, Nanjing University, Nanjing*
*2. National Center for Atmospheric Research[*], Boulder, Colorado*
*3. Department of Atmospheric Sciences, Texas A&M University, College Station, Texas*

## 1. Introduction

Although the synoptic-scale evolution of the typical midlatitude weather system is relatively well forecasted, numerical weather prediction models still have difficulties in forecasting the detailed type, track and amount of precipitation for the mesoscale systems that are of most concern to the typical user of the model's forecast. It has been hypothesized that the uncertainty associated with small-scale motions and instabilities places a fundamental limit on forecast model's ability to predict larger-scale aspects of weather systems (Lorenz 1969). While present forecast errors could of course be reduced through improvements in either the forecast models or their initial conditions, it follows from Lorenz (1969) that smaller-scale features in high-resolution forecasts may also have inherent limits of predictability.

Recent papers by Zhang et al. (2002a,b, ZSR) focusing on the "surprise" snowstorm of 24-24 January 2000 demonstrated the influence of initial errors of small scale and small amplitude on that storm. They found that initial differences grew rapidly at scales below 200 km, with doubling times of a few hours or less. The rapid error growth was dependent on moist processes and, in particular, appeared to be associated with conditional instability and moist convection (or its parameterization). In their highest-resolution experiments with an inner grid of 3.3-km horizontal resolution, the small-scale differences appeared first as differences in the timing and placement of convective cells and then spread upscale to alter the shape and location of the surface cyclone in the 36-hour forecast.

This preprint outlines recent efforts to generalize results from the "surprise" snowstorm, by investigating the suggestion of ZSR that the rapid growth of differences seen in their simulations required conditional instability and moist convection, and by attempting to understand better the mechanisms by which small-scale error spreads from convective to larger scales and thereby limits predictability on the mesoscale. These issues will be examined in the context of idealized simulations of moist baroclinic waves using the PSU/NCAR mesoscale model MM5. These simulations begin from a zonal jet in a channel to which an upper-level disturbance is added to trigger cyclogenesis.

## 2. Model description, Initial Condition and Experimental Design

The one-way nested NCAR/PSU nonhydrostatic model MM5 was used for this study(Dudhia 1993). There are two model domains (D1, D2) with 90 and 30 km grid resolution, respectively. The coarse domain employs 90 x 200 grid points with 60 vertical layers, while the number of grid points for 30-km nested domain is 160 x 280. On both domains, the experiments employ the Grell (1993) cumulus parameterization, the MRF PBL scheme (Hong and Pan 1996), the Reisner microphysics scheme with graupel (Reisner et al. 1998) and a simple radiation parameterization scheme.

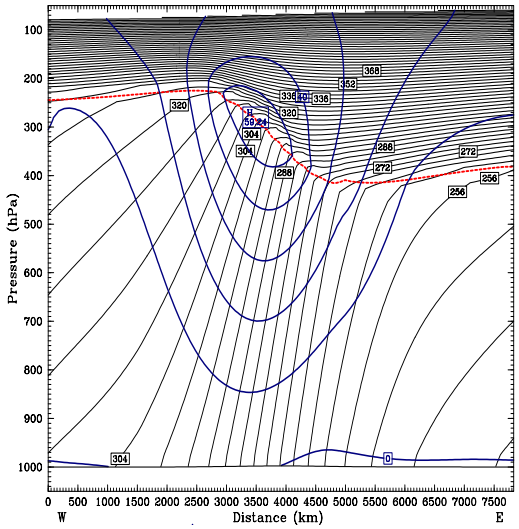


**Figure 1.** Vertical cross section of initial potential temperature (thin line) and zonal velocity (thick) for basic state. The dash line denotes the contour of PV=1PVU. Potential temperature contours are drawn every 3 K. Zonal velocity contours are drawn every 10 $ms^{-1}$.

The initial conditions are set by the following method. First we create a zonal-mean jet by specifying the location of the tropopause, with constant potential vorticity (PV) in both the troposphere and stratosphere, as in Rotunno et al. (1994). Winds and potential temperature for the jet, shown in Fig. 1, are obtained by

inverting the PV in a two-dimensional (height and latitude) plane. A localized, balanced perturbation of moderate amplitude is then added to the jet to represent the early phase of a typical midlatitude cyclogenesis. This perturbation is obtained by specifying a horizontal displacement field, calculating a PV perturbation by multiplying that displacement by the meridional gradient of PV in the jet, and finally inverting the PV perturbation for streamfunction and geopotential as in Davis and Emanuel(1991). The initial relative humidity, which varies from 90% at the lowest level to 10% above a height of 8 km, is chosen to yield a moderate amount of conditional instability in the central portion of the domain. The combination of the baroclinic jet, a balanced moderate-amplitude perturbation and the moist lower levels provides a favorable environment for strong development of the baroclinic wave.

Two numerical experiments, a control simulation and a simulation from perturbed initial conditions, were performed to investigate the growth of forecast differences. The unperturbed, control experiment was initialized as described above and run in D1 for 66 h (CTRL-D1). After 36 h, the inner domain was initialized from the solution on D1 and integrated for 24 h (CTRL-D2). Lateral boundary conditions for D2 are provided by D1, but the solution on D2 does not influence the coarser grid (e.g., "one way" nesting). The simulation from the perturbed initial conditions (PERT-D2) was performed only in D2. The perturbation to the initial conditions consists of random, Gaussian noise added to the temperature field; the noise has zero mean, standard deviation 0.2 K, and is independent at each grid point. The lateral boundary conditions for PERT-D2 are not perturbed (that is, they are identical to those of CTRL-D2).

## 3. Error growth and mesoscale predictability

*(a) Life cycle of Baroclinic Wave and Moist Convection*

Figure 2 shows the evolution and the structure of the surface temperature and sea-level pressure at the different stages of the baroclinic wave development. By 36 h, an incipient cyclone has developed out of the initial perturbation to the basic flow (Fig. 2a). At 48 h, the northeast-southwest oriented warm "conveyor belt" has appeared ahead of a strong baroclinic zone (Fig. 2b). At 48 h, a "T-bone" structure and a bent-back warm front have formed (Fig. 2c). The surface potential temperature and low-level pressure simulation present here is similar to Shapiro and Keyser's (1990) version of the life cycle of an extratropical marine cyclone.

The simulation CTRL-D2 resembles CTRL-D1 but allows for simulation of more detailed structure within the baroclinic wave. Figure 3 shows the total precipitation at 24 h for CTRL-D2 (corresponding to 60 h in CTRL-D1). Over the 24 h of simulation the surface cyclone continues to deepen and the total precipitation (6-h accumulations) continues to increase. Thus, both CTRL-D1 and CTRL-D2 provide reasonable simulations of the evolution and structure of a baroclinic wave. We will use these simulations as a testbed in which to examine the influence of moist convection on mesoscale predictability.

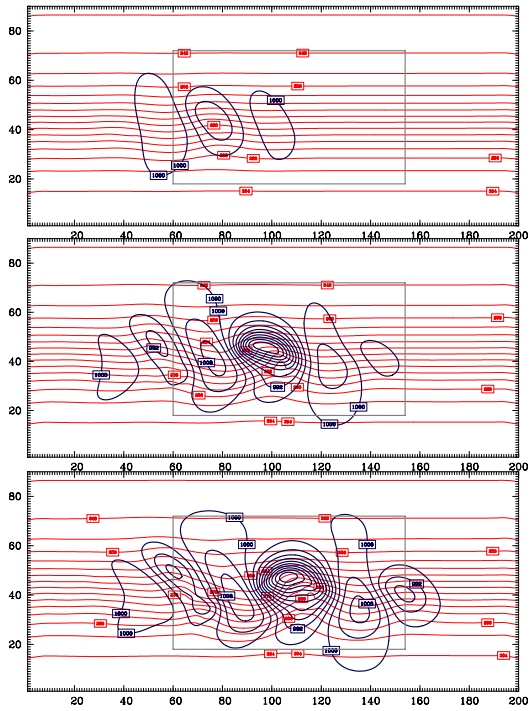


**Figure 2**. Surface potential temperature (red line) and sea-level pressure (blue line) at hours (a) 36 h, (b) 48 h, (c) 60 h. The contour interval for surface potential temperature is 4 K and sea-level pressure is 4 hPa. The inside gray box denotes the domain 2 (D2).

*(b) Error Growth in a Moist Baroclinic Wave*

Figure 4 shows the 200hPa temperature difference between CTRL-D2 and PERT-D2 at 6 h, 12 h and 24 h. After 6 h of simulation, the initial random disturbance has decayed everywhere except for a small region in the lower troposphere near the surface cyclone (not shown) and directly above that, at upper levels in the cold air in the stratosphere above the upper ridge (Fig. 4a). In both these regions, the differences increase locally over the first 6 h. At 12 h, the differences remain in a similar location relative the baroclinic wave, but the spatial scale and extent have increased (Fig. 4b). The differences have also continued to grow, with maxima of roughly 1.6 K at 12h. These trends continue through 24 h: the horizontal scale, spatial extent, and magnitude of the temperature difference are all larger than at 12 h. The maximum temperature at 200hPa is now about 13 times the initial difference.

Figure 4 also shows a single contour of CAPE from CTRL-D2, which broadly delineates the boundary between the moist, potentially unstable air to the south and drier, stable air to the north. As the baroclinic wave evolves, a tongue of large CAPE forms and extends northward toward the center of the surface low. Both the upper-level temperature differences (Fig. 4) and the convective rainfall (not shown) coincide with the northern edge of this tongue of CAPE. (The convective parameterization is active along the northern edge of the tongue, and not in the reservoir of air with higher CAPEs to the south, because the convective inhibition is minimized at the tip of the tongue.) This association of the initial error growth with conditional instability and moist convection was also found in ZSR and again supports the hypothesis that moist convection is responsible for the rapid growth of differences in the simulation.

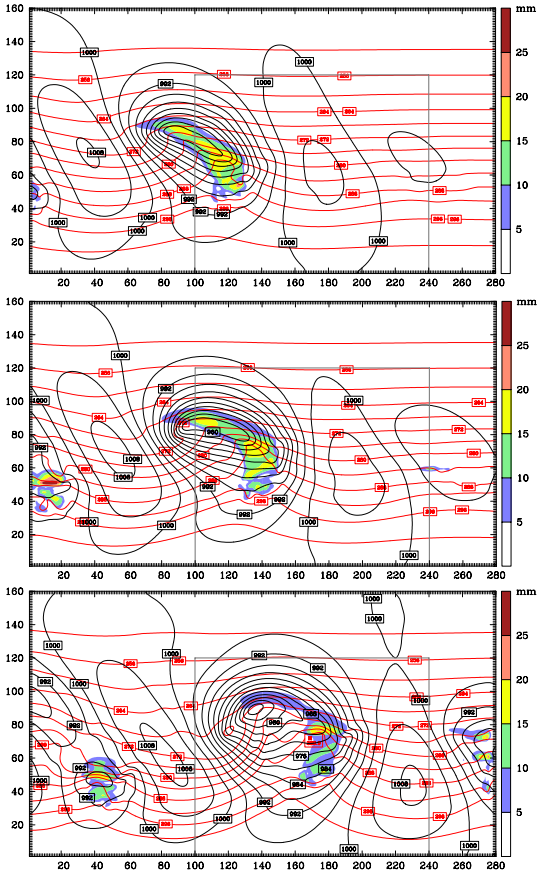


**Figure 3.** Surface potential temperature (red line), sea-level pressure (blue line) and total precipitation in the past 6 hours in the CRTL-D2 at hours (a) 6 h, (b) 12 h and (c) 24 h. The contour interval for surface potential temperature is 4 K and sea-level pressure is 4 hPa. The shading region shows the total precipitation in the past 6 h. The inside gray frame denotes the small horizontal cross section analysis regions in Fig. 4.

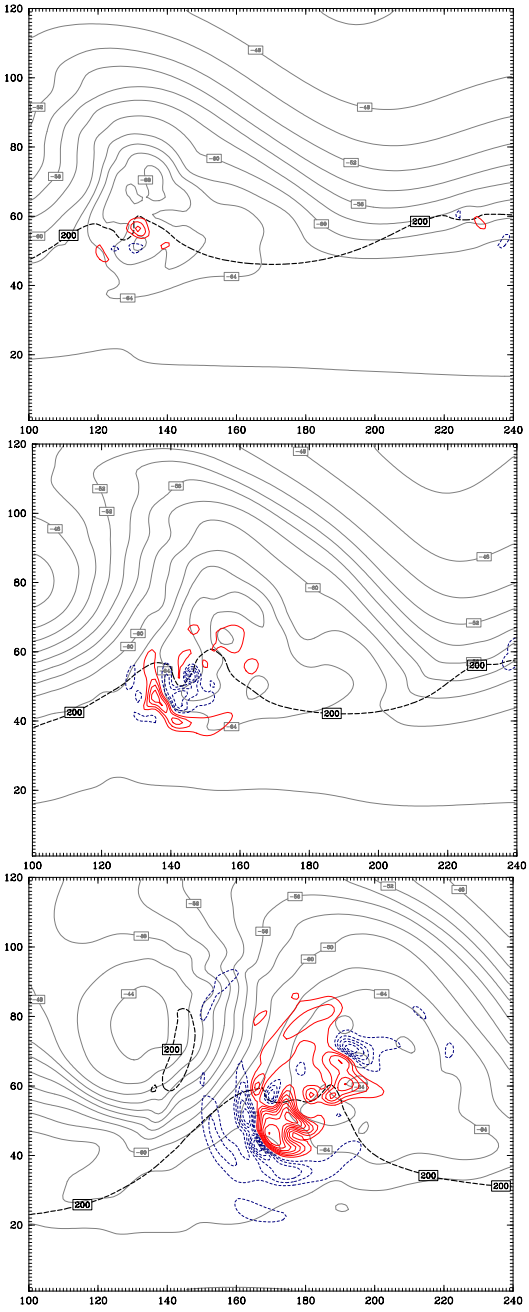

**Figure 4.** 200-hPa temperature difference between CRTL-D2 and PERT-D2 (thin line), 200-hPa temperature from CRTL-D2 (thick gray line) and the contour of CPAE=200Jkg$^{-1}$ at hours (a) 6 h, (b) 12 h, (c) 24 h. The contour intervals are 0.2 K for difference fields (negative values dash line) and 3 K for the full fields. The zero contour is suppressed

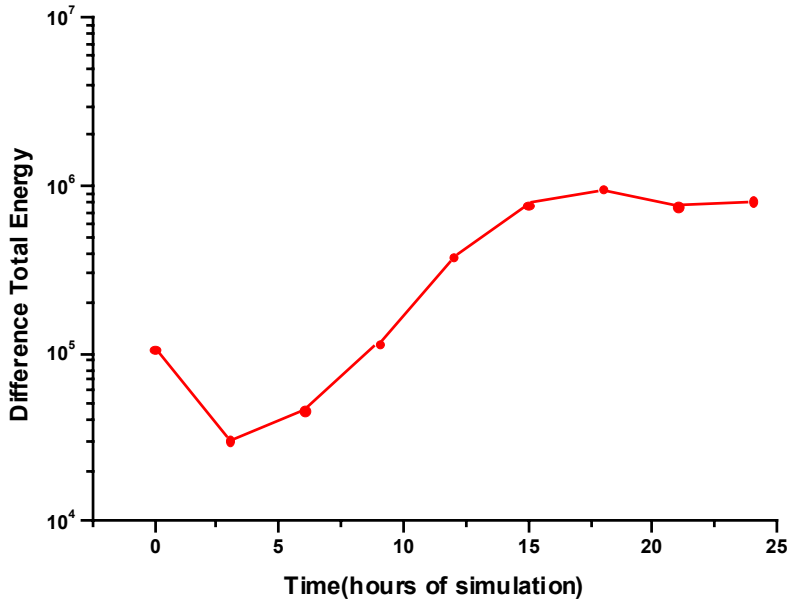


**Figure 5.** Evolution of DTE ($m^2s^{-2}$) in D2 with idealized initial perturbations.

As in ZSR, we define the difference total energy (DTE) as

$$DTE = 1/2\sum(u'_{ijk}{}^2 + v'_{ijk}{}^2 + C_p / RT'_{ijk}{}^2)$$

where $u'_{ijk}$ , $v'_{ijk}$ and $T'_{ijk}$ are the difference wind and temperature between CTRL-D2 and PERT-D2.

Figure 5 shows the evolution of DTE. After the initial 3 h, rapid growth is evident: DTE increase by more than a factor of 10 between 6 and 12 h, corresponding to an error doubling time of less than 4 hours. Comparing with the case in ZS R2002b, the error growth in this idealized baroclinic wave is relatively smaller. We believe this difference in error growth is at least partly related to the different structure of the initial random perturbation, but is also influenced by the strength of moist convection in the baroclinic wave.

## 4. Summary and discussion

Investigated here is the growth of small initial-condition differences ("errors") in simulations of large-scale baroclinic waves with regions of conditionally unstable air. Preliminary results show that error growth is initially concentrated near the developing cyclone center where moist unstable air has been lifted to its level of free convection. Difference fields show that the initially localized small-scale error grows in scale and spreads in space over the 24h integration period on the high-resolution domain; the domain-averaged error DTE doubling time is small (4h) and hence small differences grow from negligible to meteorologically significant values within 24h. We are currently investigating the dependence of the DTE on the moist instability by varying the CAPE of the base state and performing error-growth experiments. High-resolution convection-resolving experiments are planned so that the mechanics of the model-produced error growth may be discovered.

**Acknowledgments.** We are grateful to Dr. Davis Chris for useful discussion on PV inversion. This research was supported by NSF/NCAR U.S. Weather Research Program. ZMT was also supported by NSFC.

## References

Dudhia, J., 1993: *MWR*, **121**, 1493.
Lorenz, E. N., 1969: *Tellus*, **21**, 289.
Davis, C.， and K. A. Emanuel, 1991: *MWR*,119,1929
Rotunno, R., W. C. Skamarock and C. Snyder, 1994: *JAS*, **54,**3373
Zhang, F., C. Snyder and R. Rotunno, 2002a: *MWR,***130**,1617.
Zhang, F., C. Snyder and R. Rotunno, 2002b: *JAS*,in review.

Corresponding author: ZT (zmtan@ucar.edu)